Electrification of an entrainment calciner in a cement kiln system – heat transfer modelling and simulations

Ron M. Jacob Lars-Andre Tokheim

Department of Process, Energy and Environmental Technology, University of South-Eastern Norway,
{ron.jacob, Lars.A.Tokheim}@usn.no

Abstract

Carbon capture and storage may be applied to reduce the CO_2 emissions from a cement plant. However, this often results in complex CO_2 capture solutions. To simplify the capturing process, an alternative is to electrify the cement calciner. This study covers the feasibility of electrifying an existing calciner by inserting electrically heated rods in the calciner. An existing entrainment calciner in a Norwegian cement plant is used as a case study.

A model is developed to quantify the aspects concerning the feasibility of the calciner. The model first estimates the possible area of inserted rods in the available space. A mass and energy balance is then performed to estimate the heat duty of the heating rods. Further, a radiation heat transfer model is included to identify the feasibility of transferring heat from the rods to the raw meal. Finally, the model includes the design of the heating rod to estimate the required number of heating elements.

The results indicate that it is technically feasible to electrify the calciner. The total heat duty of the calciner is 77 MW, with 68 MW for meal preheating and calcining, and 9 MW for gas preheating. 2570 heating rods are required, operating at 1150 °C in the gas preheating zone and 1050 °C in the meal preheating and calcining zone. The feasible heat flux is 26-34 kW/m² for gas preheating, 35-80 kW/m² for meal preheating and 30-50 kW/m² for calcination. However, some challenges related to recuperating the heat from the gas and maintenance of the system must be studied further.

Keywords: Calcination, Electrification, Heat transfer, Resistance heating

1 Introduction

The cement industry is responsible for around 7% of the global emission of CO_2 and around 4% in the EU (IEA, 2020). The primary sources of these emissions are the combustion of fossil fuels and the decomposition of limestone ($CaCO_3 \rightarrow CaO + CO_2$). A modern cement kiln system couples these two processes, and this coupling gives a very efficient, direct-contact heat transfer.

The CO_2 emission from the system may be captured by using carbon capture and storage technologies. However, in this method, the CO_2 must be separated from other components in the flue gas, making it a complex process. A simpler solution may be to electrify the calciner. An electrified calciner will have pure CO_2 generated from the decomposition reaction, thus the need for separation from flue gas may be avoided. This method has the potential to avoid around 72 % of the CO_2 emission from the cement kiln system (Tokheim et al., 2019). However, for this to be an environmentally viable solution, the electricity must be produced from renewable sources, thereby avoiding indirect CO_2 emissions.

A suitable calciner design must be selected to electrify a calciner. Different designs may be selected, such as rotary calciners, drop tube calciners, fluidized bed calciners and tunnel calciners. The literature available on electrified calciner is sparse, and no studies of an electrified entrainment calciner have been found. The Leilac project studied a drop tube calciner with indirect heating using natural gas (Hills et. al., 2017), and this drop tube calciner may be electrified by replacing natural gas with an electrical heater (Usterud et al., 2021). A fluidized bed calciner concept using binary particles has also been studied (Samani et. al., 2020).

In this study, electrification of an existing calciner operating in the entrainment mode is used in a case study. This will provide a reference case to which other potential calciner designs may be compared when it comes to electrification.

This work aims to study the possibility of electrifying the entrainment calciner by inserting heating rods in it. Such a concept may make it easy for the cement industry to quickly transition to an electrically heated calciner without making significant changes to the existing calciner geometry. Such a study has not been published before to the best of authors' knowledge.

2 System description

An entrainment calciner operating in a Norwegian cement plant, producing 1 Mt of clinker per year, is considered for electrification in this study. A comparison of the existing calciner and an electrified version of this calciner are shown in Figure 1.

The existing calciner (cf. the left-hand side of Figure 1) has five main parts; a downdraft flash calciner with a burner, a mixing chamber, a tube calciner, a swirl chamber and gas duct connections to cyclone separators (Tokheim, 2006).

The fuel mix (coal, refused derived fuel, solid hazardous waste and animal meal) is fed into the downdraft burning-chamber where it is mixed with tertiary air and preheated meal. The fuel ignites and provides energy for calcination of the preheated meal. The meal swirls around the burner wall and protects it from too high temperature generated by the burning fuel. The meal is then transported to the mixing chamber where it mixes with high temperature kiln gas. The kiln gas provides additional energy needed for meal calcination and also enough energy to entrain the meal through the tubular calciner (the "Pyroclone") towards the swirl chamber (the "Pyrotop"), which improves the burnout of fuel particles. The mixture of gas and meal is then transported to cyclone separators, where the calcined meal is sent to the rotary kiln for further processing, whereas the gas is used for preheating of meal in cyclone preheater tower (Tokheim, 2006). The dimensions of the reference calciner used for calculations are summarized in Table 1.

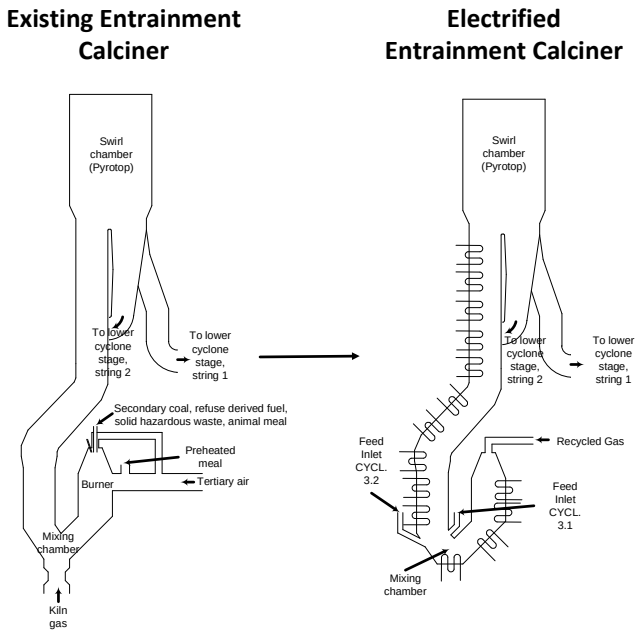

Figure 1: Existing (left) vs electrified entrainment calciner (right)

Table 1. Dimensions of the reference calciner geometry

Dimensions	Symbol	Value
Diameter of the tubular calciner [m]	D_C	3.74
Length of the gas preheater section [m]	L_{GP}	7
Length of the calciner section after meal feeding [m]	L_C	50.2

The existing calciner may be converted to an electrified calciner by making the following changes (Figure 1, right-hand side):

1. Cutting the supply of kiln gas
2. Cutting the supply of fuel, air and preheated meal in the burner
3. Moving the meal inlets to a position right above the mixing chamber
4. Feeding recycled CO_2 (required for particle entrainment) at the top of the combustion chamber
5. Inserting heating rods in the combustion chamber and the mixing chamber to provide energy for preheating of the recycled gas
6. Inserting heating rods along the tube calciner geometry to provide energy for calcination

The kiln gas and the tertiary air will bypass the electrified calciner (Figure 1, left-hand side) and will instead be mixed and lead to the preheater tower (not shown in the figure) for meal preheating, so that the rest of the kiln system is unaffected by the calciner modification.

3 Model development

The modelling combines a mass and energy balance of the calciner with a geometric model for insertion of heating rods, a model for heat transfer from the heating rods and design of an appropriate heating element. This section covers these four aspects of the modelling work.

3.1 Heating element design

Resistance heating is a relatively simple technology for electricity-based heating. The heat is produced when an electric current (I) passes though a resistor (the heating element) with a certain resistance (R). The produced heating rate ($\dot{q}_e$) may be quantified as,

$$\dot{q}_e = I^2 R = VI \qquad (1)$$

Here, V is the voltage drop over the heating element.

The resistance of the heating element (R) is further given by,

$$R = \rho_e \frac{4 l_e}{\pi {d_e}^2} \qquad (2)$$

Here, ρ_e is the resistivity of the heating element, l_e is the length of the heating element and d_e is its diameter (assuming it is a wire).

The resistivity of the heating element is dependent on the resistor material. A range of materials is available in the market. They include metallic alloys such as nichrome, Kanthal wires, and non-metallic elements such as silicon carbide and molybdenum disilicide.

Metallic alloys are generally recommended for temperature ranges of 1200-1400 °C, whereas non-metallic materials are recommended for higher temperatures, i.e. the range 1600-1900 °C (Lupi, 2017).

The calciner will operate between 900 and 1000 °C. Hence, metallic alloys are considered in this work. The maximum operating temperature of some metal alloys are shown in Figure 2, whereas the resistivity as a function of temperature is shown in Figure 3.

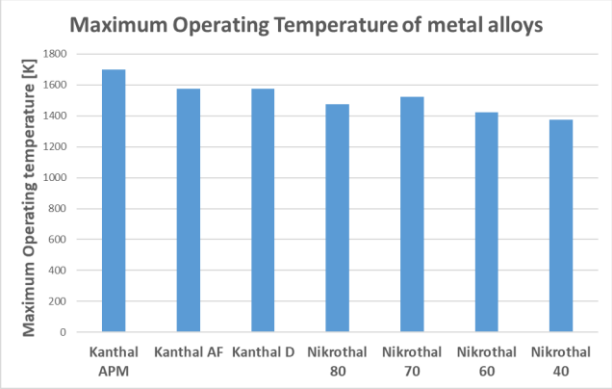

Figure 2: Maximum operating temperatures of some metal alloys used for resistance heating

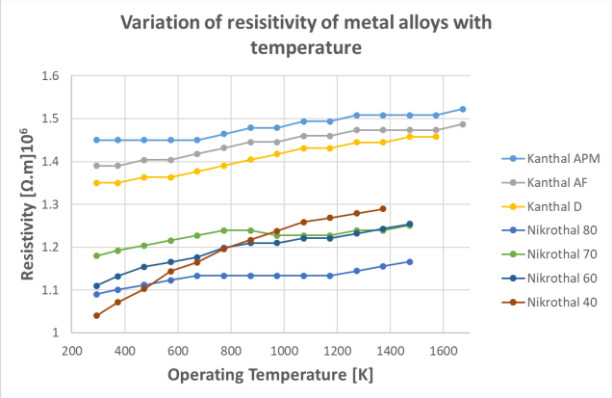

Figure 3: Variation of resistivity with temperature for some metal alloys

The heating elements may be mounted into the furnace with various support systems. In this study, spiral winding of heating elements on a ceramic tube is considered, referred to as heating rods in the study. The schematic of this system is shown in Figure 4.

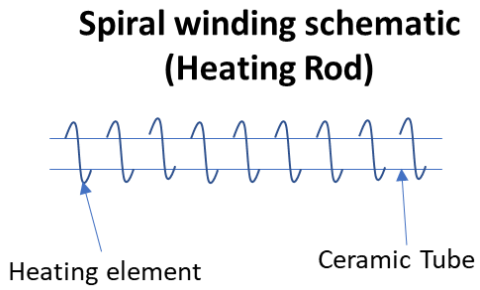

Figure 4: Spiral-winding schematic (heating rod)

The recommended value for the diameter of the heating element (d_e) is 2.0 – 6 .5 mm and that of the ceramic tube diameter (D_R) is $D_R = (12 - 14) \times d_e$ (Kanthal, 2020). In this study, the diameter of the heating element (d_e) is assumed to be 4 mm, and the ceramic tube diameter (D_R) is assumed to be 50 mm.

3.2 Heating rod insertion model

A model is developed to predict the area occupied by the inserted heating rods (A_R). In general, if this area is large, the contact between the heating surface and the meal will be large, leading to a higher heat transfer rate. However, if the area is too large, by inserting too many rods, then the space between the rods might be too small, which will affect the structural integrity of the calciner. A model is developed by assuming a defined heating rod arrangement and using the fraction of axial and radial length occupied by heating rods (f_C) and the diameter of the heating rods (D_R) as input parameters. The proposed heating rod arrangement is shown in Figure 5.

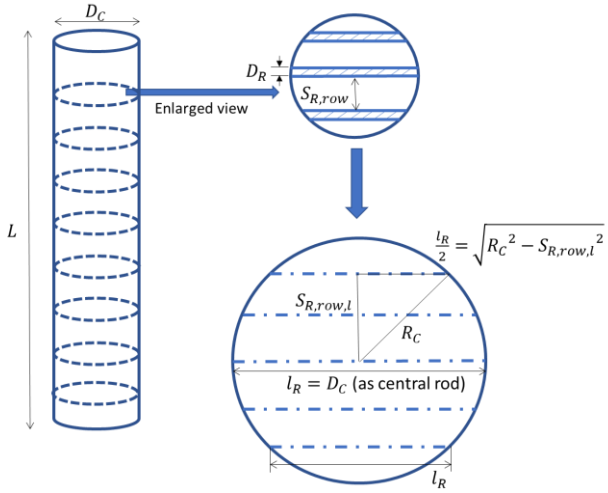

Figure 5: Heating rod design pattern

The fraction f_C is directly related to the heating rod area. Increasing this fraction will provide more space for the placement of heating rods, which in turn will increase the total area of the heating rods.

The total length occupied by the heating rods is given by,

$$f_C L = D_R N_{col} \tag{3}$$

Here, L is the length of the section, equal to L_{GP} in the gas preheating section and equal to L_C in the meal section. N_{col} is the number of columns in the axial (gas flow) direction. Rearranging the equation,

$$N_{col} = \frac{f_C L}{D_R} \tag{4}$$

To simplify calculations in the radial direction, one rod is assumed to go through the center of the calciner (the length of this rod is equal to calciner diameter, D_C), whereas the other rods are placed between the center rod and the wall in both directions, as shown in Figure 5. To

facilitate visualization, only a few rods are shown in the figure.

The number of rods in each radial direction ($N_{R,row,m}$) is given by,

$$N_{R,row,m} = \frac{f_C R_C}{D_R} \quad (5)$$

Here, R_C is the radius of calciner. The number of heating rods per rows is given by,

$$N_{R,row} = \left(2 \times N_{R,row,m}\right) + 1 \quad (6)$$

The total number of rods is further be given by,

$$N_R = N_{R,row} \times N_{col} \quad (7)$$

If the spacing between the rods in a row ($S_{R,row}$) is equal, it can be determined by,

$$S_{R,row} = \frac{R_C - \left(N_{R,row,m} \times D_R\right)}{N_{R,row,m} + 1} \quad (8)$$

The length of each rod (l_R) in the radial direction is, however, different for each rod. This length can be derived from Pythagoras' theorem as shown in Figure 5 and is given by,

$$l_R = 2 \times \sqrt{{R_C}^2 - {S_{R,row,l}}^2} \quad (9)$$

Here $S_{R,row,l}$ is the actual spacing distance of each rod from the central rod (as also shown in Figure 5).

An effective rod length ($l_{R,eff}$) is then calculated by taking the average over all possible lengths in the calciner. The total area occupied by the inserted rods (A_R) can thus be given by,

$$A_R = N_R \times \pi D_R l_{R,eff} \quad (10)$$

3.3 Heat and mass balance

To simplify the calculations, the modified calciner may be divided into three zones.

1. **Gas preheating zone:** The gas is preheated to the calcination temperature in this zone.
2. **Meal preheating zone:** The meal is preheated to the calcination temperature in this zone.
3. **Meal calcining zone:** The meal gets calcined ($CaCO_3$ → $CaO + CO_2$) in this zone.

The simplified reactor model is shown in Figure 6.

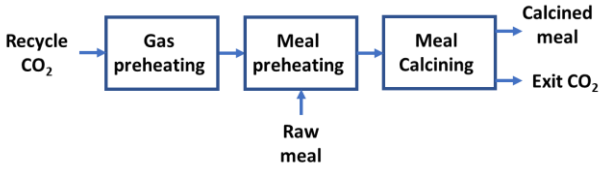

Figure 6: Different zones used in the heat and mass balance

The entrainment velocity in existing calciners may vary between 10-20 m/s (Becker et al., 2016), while in some calciners, this gas velocity may be as low as 5-7 m/s. In this study, the entrainment velocity is assumed to be 7 m/s. The impact of changing this is presented in the results. Other assumptions are summarized in Table 2.

The calcination temperature (T_{calc}) is relatively high (914 °C) compared to regular calciners. This is because the gas in the electrified calciner is pure CO_2, so a higher temperature is required to generate a CO_2 equilibrium pressure (Stanmore and Gilot, 2005) higher than the partial pressure in the calciner (~1 atm). The temperature of the recycled gas ($T_{in,g}$) is based on a previous study on CO_2 heat utilization (Jacob, 2019). The other values in the table are based on a previous calciner electrification study applying the same kiln system as a design basis (Tokheim et al., 2019).

Table 2: Assumptions for heat and mass balance

Section	Parameter	Symbol	Value
General assumptions	Entrainment velocity	v_C	7 m/s
	Calcination temperature	T_{calc}	914°C
	Weight fraction of CaCO3 in raw meal	w_{CaCO3}	0.77
Gas preheating	Inlet temperature of recycle gas	$T_{in,g}$	470°C
	Outlet temperature of recycle gas	$T_{out,g}$	914°C
Meal preheating	Mass flow rate of raw meal	$\dot{m}_{PHM}$	210 ton/hr
	Inlet temperature of raw meal	$T_{in,PHM}$	658°C
Meal calcination	Enthalpy of calcination	H_{calc}	-3.6 MJ/kgCO_2
	Enthalpy of other reactions in the calciner	$H_{calc,other}$	0.3 MJ/kgCO_2
	Calcination degree	f_{calc}	0.94

The mass flow rate of CO_2 ($\dot{m}_{CO2,C}$) inside the calciner may be calculated from entrainment velocity by,

$$\dot{m}_{CO2,C} = \rho_{CO2} A_C v_C \quad (11)$$

Here, ρ_{CO2} is the density of gas calculated from the ideal gas law, A_C is the cross-sectional area of the calciner and v_C is the velocity of gas inside the calciner (entrainment velocity). The mass flow of CO_2 ($\dot{m}_{CO2,calc}$) produced from calcination reaction is calculated by,

$$\dot{m}_{CO2,calc} = \dot{m}_{PHM} w_{CaCO3} \frac{M_{CO2}}{M_{CaCO3}} \frac{1}{f_{calc}} \quad (12)$$

Here, M_{CO2} is the molecular mass of CO_2 and M_{CaCO3} is the molecular mass of $CaCO_3$.

The mass flow rate of recycling CO2 ($\dot{m}_{CO2,recyc}$) can thus be determined by,

$$\dot{m}_{CO2,recyc} = \dot{m}_{CO2,C} - \dot{m}_{CO2,calc} \quad (13)$$

The heat required to heat the CO_2 (q_{GP}) in the gas preheater section is given by,

$$q_{GP} = \dot{m}_{CO2,recyc} C_{p,CO2} \left(T_{in,g} - T_{out,g}\right) \quad (14)$$

Here $C_{p,CO2}$ is the heat capacity of the gas given by a polynomial equation (Green, Perry, 2008),

$$C_{p,CO2} = C1 + C2\left[\frac{C3/T}{sinh\,(C3/T)}\right]^2 + C4\left[\frac{C5/T}{cosh\,(C5/T)}\right]^2 \times \frac{M_{CO2}}{1000}\, J/kg.K \quad (15)$$

Here, C1 = 29370, C2 = 34540, C3 = 1428, C4 = 26400 and C5 = 588 (units are skipped here for simplicity).

The heat required in the meal preheating section (q_{MP}) is given by,

$$q_{MP} = \dot{m}_{PHM} C_{p,PHM} \left(T_{in,PHM} - T_{calc}\right) \quad (16)$$

Here $C_{p,PHM}$ is the heat capacity of preheated meal and is equal to 1260 J/(kg·K) (Samani, 2020).

The heat required in the meal calcination (q_{MC}) is given by,

$$q_{MC} = q_{MC,out} - q_{MC,in} - q_{cal} - q_{cal,other} \quad (17)$$

Here, $q_{MC,out}$ is the outlet heat from calcination section, which is given by the sum of heat in the calcined meal and the outlet gas. $q_{MC,in}$ is the heat in the inlet raw meal after meal heating and the heat in the inlet gas. q_{cal} is the heat required to calcine the meal and $q_{cal,other}$ is the heat from other meal reactions (Samani, 2020).

3.4 Heat transfer coefficient

Convection and radiation are the main heat transfer modes in an entrainment calciner. However, at temperatures higher than 600 °C, the heat transfer by radiation is much more dominant than the heat transfer by convection (Lupi, 2017). Since heat transfer from radiation is dominant, this study covers radiation only, and a network modelling approach is applied.

A pure CO_2 environment is expected inside the calciner due to recycled CO_2 and CO_2 formed in the calcination reaction. CO_2 emits and absorbs radiation over a wide temperature range, as it is a polar gas (Incropera et. al., 2017). The radiating property of CO_2 complicates the radiation modelling as it participates in radiation heat transfer along with the particles, the calciner wall and the heating rods. This is handled by using a network modelling approach in this work, as described below.

The total radiation heat transfer (q_{rad}) from surface i to N surfaces (each surface denoted by j), and assuming the surfaces to be grey, is given by (Incropera et. al., 2017),

$$q_{rad} = \sum_{j=1}^{N} q_{ij} = \frac{E_{b,i} - J_i}{(1-\varepsilon_i)/\varepsilon_i A_i} = \sum_{j=1}^{N} \frac{J_i - J_j}{\left(A_i F_{ij}\right)^{-1}} \quad (18)$$

Here, q_{ij} is the heat transferred from surface i to another surface denoted by j subscript, $E_{b,i}$ is the total emissive power for a black surface i, J_i is the radiosity which accounts for all radiant energy leaving the surface i, ε_i is the emissivity of the surface i, A_i is the area of surface i and F_{ij} is the view factor from surface i to surface j. The formulated network equation is visualized in Figure 7.

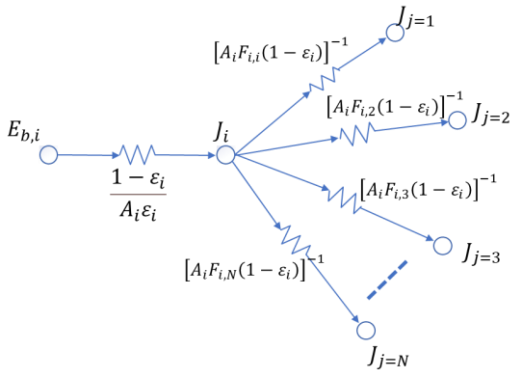

Figure 7: Schematic of a network model with total radiative heat transfer from surface i to other surfaces

3.4.1 Gas preheating

In the gas preheating section, the heat is exchanged between the gas (subscript g), the heating rods (subscript R) and the calciner wall (subscript w). The wall is well insulated, so heat loss is neglected. Then the wall can be assumed to be a re-radiating surface, i.e., it re-radiates all the incident heat. The resulting network of this system is shown in Figure 8. Approximate values of emissivities and view factors are given in Table 3.

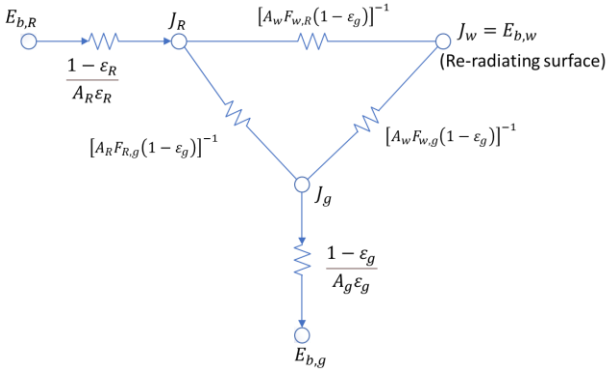

Figure 8: Network model of radiative heat transfer in the gas preheating zone

Table 3: Assumed parameters in the network model for radiation heat transfer in the gas preheating zone

Parameter	Symbol	Value
Emissivity of CO_2	ε_g	0.15
Emissivity of heating rod	ε_R	0.7
View factor from rod to wall	$F_{w,R}$	0.5
View factor from rod to gas	$F_{R,g}$	1
View factor from wall to gas	$F_{w,g}$	1

The emissivity of CO_2 (ε_g) is dependent on the partial pressure of CO_2, the mean beam length and the gas temperature (Hottel and Egbert, 1940). An approximate emissivity of CO_2 is read from Hottel's chart, which correlates these factors to the emissivity of the gas.

The emissivity of the heating rod (ε_R) was approximated based on literature (Kanthal, 2020). There are some uncertainties related to the rod-wall view factor between ($F_{R,w}$). This factor may lie between 0 and 1. An approximate value of 0.5 is chosen, and a sensitivity study on this parameter is presented in the results. The rod-gas and wall-gas view factors should be 1 as the gas is fully visible to these surfaces.

3.4.2 Meal preheating and calcining

In the preheating and calcination section, the heat is exchanged between the gas (subscript g), the heating rods (subscript R), the raw meal particles (subscript p) and the calciner wall (subscript w). The wall can be assumed to be re-radiating if no heat loss present. The gas is also assumed to be re-radiating as the gas has already been heated to the calcination temperature, and now, it is just re-radiating all the incident heat directly to the raw meal particles, the wall and the heating rods. The resulting network is shown in Figure 9.

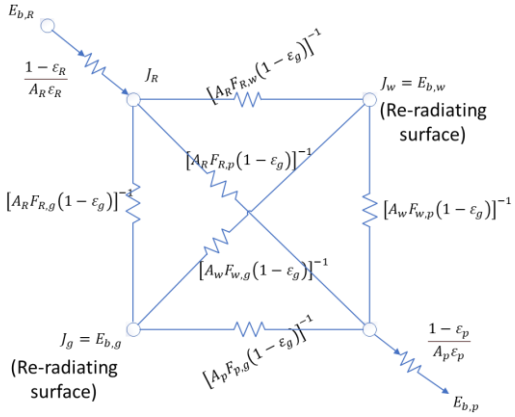

Figure 9: Network model of radiative heat transfer in meal preheating and calcining

Approximate input values are given in Table 4. There are some uncertainties related to the area of the particles and the view factors. The higher the area of particles, the higher is the heat transfer. To be on a conservative side, the smalles probable particle area is estimated qualitatively, and then a sensitivity study is done using higher values. Assuming a void fraction (ε_m) of 0.99, the bulk density (ρ_{bulk}) of the particle inside the calciner is given by,

$$\rho_{bulk} = \rho_P \times (1 - \varepsilon_m) \quad (19)$$

Here, ρ_P is the particle density and is assumed to be 2700 kg/m^3. The calciner is assumed to be a cylinder and the volume of the calciner is calculated using the calciner dimensions (Table 1). The mass of particles inside the calciner is calcuted using bulk density and the volume of calciner. The specific surface area of traditional limestone is 1 – 10 m²/g (Stanmore and Gilot, 2005). Using the mass of particles and the specific area of a traditional limestone, the total particle area (A_p) is higher than 10^6 m^2. This value is taken as a base case, and a sensitivity study is later performed with a higher particle area. The rod-particle view factor ($F_{w,p}$) and the wall-particle view factor ($F_{w,p}$) should both be close to 1 as in case of dusty flow inside the calciner, the particles are fully visible to the rod and the wall. Due to the presence of this dust, the rod-wall view factor should be low (close to 0). Based on these arguments, approximate values are selected, and a sensitivity analysis is done on the results.

Table 4: Assumed parameters in the network model for radiation in the preheating and calcining zone

Parameter	Symbol	Value
Emissivity of CO_2	ε_g	0.15
Emissivity of heating rod	ε_R	0.7
Emissivity of particles	ε_p	0.7
Area of particles	A_p	10^6
View factor from rod to wall	$F_{R,w}$	0.1
View factor from rod to particle	$F_{R,p}$	0.8
View factor from wall to particle	$F_{w,p}$	0.8
View factor from particle to gas	$F_{p,g}$	1
View factor from rod to gas	$F_{R,g}$	1
View factor from wall to gas	$F_{w,g}$	1

4 Results and discussions

Simulations are performed with the model described in Section 3. The results from the heating rod insertion model are presented in Figure 10. The results show the boundary limits of the rod area of in the gas preheating zone ($A_{R,GP}$), the meal preheating zone ($A_{R,MP}$) and the meal calcination zone ($A_{R,MC}$). The minimum area of the rod should be at least the area of calciner geometry ($A_{GP}/A_{MP}/A_{MC}$). The maximum area is the area at which the minimum possible spacing between the heating rod is reached in each zone ($A_{GP,Smin}/A_{MP,Smin}/A_{MC,Smin}$). The minimum spacing between rods is assumed to be 2.5 times the

rod diameter. This information is used to estimate the heat transfer from radiation.

The heat transfer results from the heat and mass balance in each zone are shown in Figure 11. 8.7 MW of heat is required to preheat the recycled CO_2. This heat might be difficult to recuperate and may result in significant heat losses from the system (Jacob, 2019). If the entrainment velocity is higher than the assumed value (7 m/s), the heat loss will be even higher. A sensitivity analysis of this heat duty by varying the entrainment velocity is shown in Figure 12. The results clearly show the importance of minimizing the gas recycling.

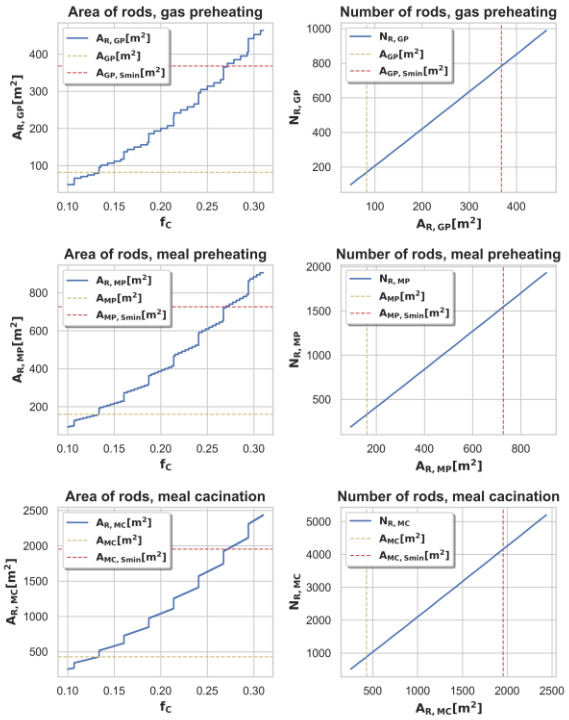

Figure 10: Result from the heating rod insertion model

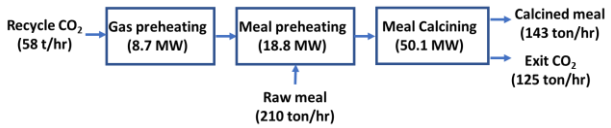

Figure 11: Results from the heat and mass balance calculations

The heat transfer results for each calciner section are shown in Figure 13. The results are plotted for three different heating rod temperatures in each case. The band represents the sensitivity to the uncertainties discussed in Section 3.4. Monte-Carlo simulations are performed on the uncertainties to find the maximum and minimum values of heat transfer given the uncertainties. The dotted line in Figure 13 represents the required heat duty in each section of the calciner calculated from the heat and mass transfer calculations (cf. Figure 11).

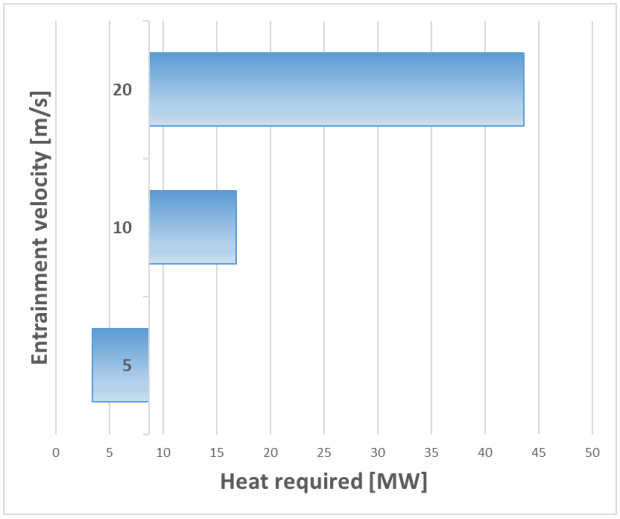

Figure 12: Sensitivity analysis on gas preheating duty (potential heat loss)

The results in Figure 13 show that it is technically feasible to transfer heat through the radiation mechanism. The total number of rods required can be read by combining Figure 10 and Figure 13. In the gas preheating section, the temperature of the rod should be 1150 °C, and the number of required heating rods required at the feasibility point will be around 450. In the meal preheating section, the heat may be transferred at 1050 °C with around 420 rods at the feasibility point. In the meal calcining section, the heat can also be transferred at 1050 °C with around 1700 heating rods at the feasibility point. The total number of required heating rods is around 2570.

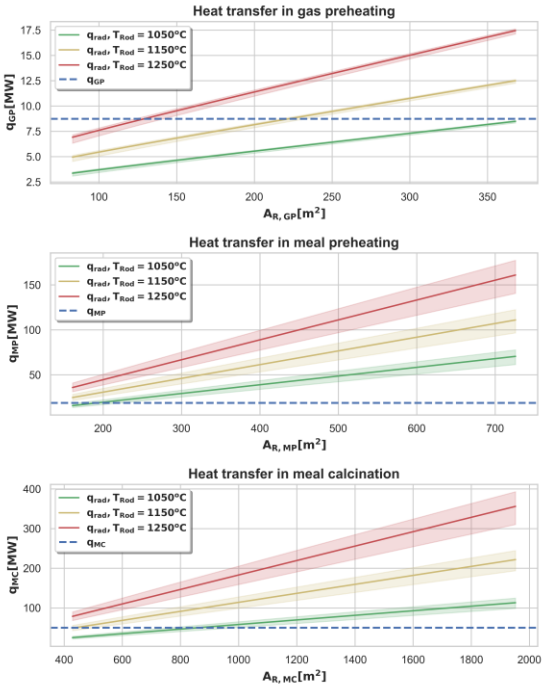

Figure 13: Heat transfer results from each calciner section

A range of feasible heat fluxes are obtained by dividing heat rate with rod area. This result is then utilized to find a heating element design and estimate the mass of the heating element required. The mass of heating elements in the feasible range of heat fluxes in different calciner zones is shown in Figure 14. The lowest mass required in the feasible range of operating calciner is found by using Kanthal APM heating elements.

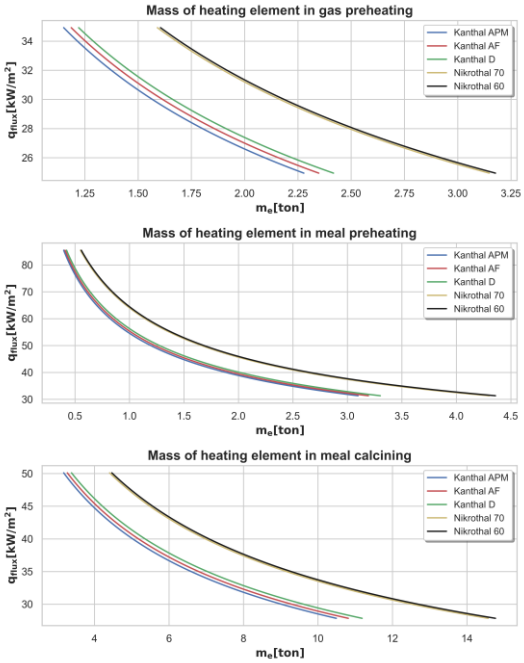

Figure 14: Mass of elements required in the feasible range of operating calciner

5 Conclusion

Electrification of the existing calciner appears to be technically feasible. There is sufficient volume available in the calciner, and there is enough calciner shell surface area available, to insert the number of heating rods that are required to provide the heat and calcine the meal, i.e., about 2570 heating elements operating with surface temperature of 1150 °C in gas preheating zone and 1050 °C in meal preheating and calcining zone.

The total heat transferred from the electrical heating elements to the meal is 69 MW and the total heat transferred is 78 MW. The gas preheating section may operate feasibly with a heat flux of 26-34 kW/m². The meal preheating section may operate feasibly with a heat flux of 35-80 kW/m², and the meal calcining section should feasibly operate with heat flux of 30-50 kW/m². At higher heat fluxes, the heat transfer from radiation will not be enough to transfer the heat to the gas or the raw meal. At lower heat fluxes, the spacing between the heating rods will be so small that it will affect the structural integrity of the calciner. Moreover, a lower heat flux also means a higher heating element cost as the mass of the elements will increase. The mass of Kanthal APM elements, which have the highest heat flux, is around 5 tons, and the mass of the elements with the lowest heat flux is around 15 tons.

The results, however, also indicate some challenges. The gas flow rate required to entrain the raw meal may lead to high flow of energy out of the calciner, and it may be a challenge to recuperate all the heat from this

One may think of adding a fan operating at high temperature to recycle the gas at 900 °C, thereby avoiding the heat exchange. However, additional studies must be performed to check the feasibility of this. The results also indicate that a large number (at least 2120) of rods and a high mass of heating elements (at least 4 are required. The particles may flow at a high velocity in this region which may cause abrasion, erosion, and element breakage. So, maintenance may become a challenge logistically due to a large number of heating rods (finding the damaged heating rod), and economically due to the high mass of heating elements (erosion of elements). Additional studies on these aspects must be performed to find detailed economic and logistic challenges.

Thus, the results indicate that electrification of an entrainment calciner is theoretically possible. However, there are some challenges to address with this concept. One way to address the challenge may be to study other calciner systems where it is easier to avoid these challenges.

Acknowledgments

This study was carried out as part of the research project Combined calcination and CO_2 capture in cement clinker production by use of CO_2-neutral electrical energy – Phase 2". Gassnova and Norcem are greatly acknowledged for funding this project. The technical recommendations from representatives of Kanthal, Cementa, IFE and SINTEF are also acknowledged.

References

Simon Becker, Robert Mathai, Kristina Fleiger, Giovanni Cinti. Status report on calciner technology. *CEMCAP*, Rev. 2, 2016.

Don W. Green, Robert H. Perry. Perry's chemical engineers' handbook, *McGraw-Hill*, Ed. 8, 2008.

H.C. Hottel, R.B. Egbert, The radiation of furnace gas. *ASME*, 1940.

Technology Roadmap - Low-Carbon Transition in the Cement Industry. 2018.

Frank P. Incropera, David P. Dewitt, Theodore L. Bergman, Adrienne S. Lavine. Principles of heat and mass transfer. *John Wiley & Sons*, Global edition, 2017.

Ron M. Jacob. Gas-to-gas heat exchanger for heat utilization in hot CO_2 from an electrically heated calcination process, *Master's thesis*, USN, 2019.

Kanthal. Resistance heating alloys and systems for industrial furnaces, *Product overview*, 2020.

Sergio Lupi. Fundamentals of Electroheat – Electrical technologies for process heating. *Springer*, 2017

Martin H. Usterud, Ron M. Jacob, Lars-Andre Tokheim. Modelling and Simulation of an electrified drop-tube calciner. Submitted to the *SIMS conference*, 2021.

Nastaran Ahmadpour Samani. Calcination in an electrically heated bubbling fluidized bed applied in calcium looping, *Master's thesis*, University of South-Eastern Norway, 2020.

Nastaran Ahmadpour Samani, Chameera K. Jayarathna, Lars-Andre Tokheim. CPFD simulation of enhanced cement raw meal fluidization through mixing with coarse inert particles, Linköping Electronic Conference Proceedings, 176:57 (Proceedings of the 61st SIMS, September 22nd - 24th, virtual conference), pp. 399–406, 2020, https://doi.org/10.3384/ecp20176399B. R. Stanmore, P. Gilot. Review – Calcination and carbonation of limestone during thermal cycling for CO_2 sequestration, *Fuel process technology*, 86, pp. 1707-1743, 2005.

Lars-André Tokheim. The impact of staged combustion on the operation of a precalciner cement kiln, *PhD dissertation*, Norwegian University of Science and Technology / Telemark University College, 1999

Lars-André Tokheim. Kiln system modification for increased utilization of alternative fuels at Norcem Brevik, *Cement International*, 4, pp. 1-8, 2006

Lars-André Tokheim, Anette Mathisen, A., Lars E. Øi, Chameera Jayarathna, Nils H. Eldrup and Tor Gautestad. Combined calcination and CO_2 capture in cement clinker production by use of electrical energy, *SINTEF proceedings*, 4, pp 101-109, 2019

Thomas P. Hills, Mark Sceats, Daniel Rennie, Paul Fennell, LEILAC: Low cost CO_2 capture for the cement and lime industries. Energy Procedia, Vol. 114, pp. 6166-6170, 2017.